Active Polarimetry for Orbital Debris Identification

Michael C. Pasqual
Department of Aeronautics and Astronautics, Massachusetts Institute of Technology

Kerri L. Cahoy
Department of Aeronautics and Astronautics, Massachusetts Institute of Technology

Eric L. Hines
M.I.T. Lincoln Laboratory

ABSTRACT

We present the results of polarimetric measurements that may help remotely identify orbital debris fragments, thereby extending current space surveillance capabilities. A bench-top polarimeter (λ = 1064 nm) was used to experimentally determine the polarimetric Bidirectional Reflectance Distribution Function (BRDF) of several common spacecraft materials and coatings, including glossy white paint, matte black paint, black Kapton®, silver Teflon®, aluminum, and titanium. Analysis of these measurements allowed us to estimate each material's Mueller matrix and associated polarimetric properties as functions of the incident angle and (bistatic) in-plane scatter angle. Results revealed notable trends in the materials' polarimetric signatures. Specifically, the materials exhibited mostly weak diattenuation ($D < 0.5$) in all scatter directions, except for Kapton® and the two paints ($D > 0.5$ in the forward scatter direction). In terms of retardance (R), silver Teflon® exhibited a finite range of values (R = 30 to 120º) in all directions, while the other materials acted as mirrors (R = 180º) in the back scatter direction and had the full range of behavior (R = 0 to 180º) in the forward scatter direction. Finally, in terms of depolarization power (Δ), glossy white paint was a nearly perfect depolarizer ($\Delta \approx 1$) in the back scatter direction, but sharply lost depolarization power ($\Delta = 0$) at specular reflection. All other materials were mostly weak depolarizers ($\Delta < 0.5$) in all scatter directions. These experimental findings may be used to develop requirements for a polarimetric laser radar that can interrogate debris fragments, identify their constituent materials, and infer their masses and other characteristics of interest.

1. INTRODUCTION

Man-made orbital debris is a real and growing problem for the continued development and operation of spacecraft [1, 2]. The increasing risk of collisions among debris and active spacecraft is changing the way mankind approaches the space enterprise, especially in the Low Earth Orbit (LEO) environment. Now more than ever, space agencies and organizations must consider ways to remove debris already in orbit, mitigate the creation of additional debris, and protect satellites from collisions through shielding and avoidance maneuvers [3, 4, 5]. Any protection, mitigation, or removal strategy will require an accurate characterization of the space debris population, including the ephemerides, sizes, number densities (i.e., number of fragments per volume), and masses of debris fragments. Historically, radars and passive optical telescopes have provided the vast majority of data on existing debris. However, in the last two decades, several groups have designed and built ground-based laser radars for the primary purpose of tracking orbital debris [6, 7, 8, 9, 10]. The ultimate goal of these systems is to track debris fragments that are 1 to 10 cm in size with 1 meter accuracy. Such small debris can cause catastrophic damage in a collision, yet cannot be tracked reliably with other techniques because of their small cross sections and orbital instability [11].

In addition to providing an enhanced tracking capability, the advent of laser radars for space surveillance also presents an opportunity to glean information about orbital debris through active polarimetric measurements [8]. By exploiting the unique polarimetric signatures of man-made materials, active polarimetry may help determine a debris fragment's material type and (by inference) its mass and other important characteristics.

To explore the potential value of active polarimetry for space surveillance, we implemented a bench-top polarimeter (λ = 1064 nm) to measure the Bidirectional Reflectance Distribution Function (BRDF) of materials and coatings

commonly found on man-made satellites and debris. The BRDF of each material was measured as a function of the polarization state of the incident and reflected light, thereby allowing us to compute the material's Mueller matrix as a function of the incident and scatter angles. We then decomposed the Mueller matrices to derive their underlying polarimetric properties, particularly diattenuation (D), retardance (R), and depolarization power (Δ). Our results revealed that spacecraft materials have notable trends in their polarimetric signatures. Pending further analysis, our findings suggest that a polarimetric laser radar may be able to make non-resolved measurements to help remotely identify and characterize debris fragments.

The remainder of this paper is organized as follows. Section 2 introduces the fundamentals of our approach, including the technical details of active polarimetry and the optical properties we seek to exploit. Section 3 describes our implementation and verification of a bench-top polarimeter. Section 4 summarizes the results of our measurements of the polarimetric BRDF and subsequent Mueller matrices and polarimetric properties of several spacecraft materials. Section 5 discusses the implications of these experiments for the viability of active polarimetry for orbital debris characterization. Section 6 concludes with our outlook for future work in this promising area of research.

2. APPROACH

Polarimetry is a technique by which one measures the polarization state of light reflecting off a target or target scene [12, 13]. Because different materials often have unique polarimetric signatures, polarimetry has proven useful for many applications in target detection and image contrast enhancement. As illustrated in Figure 1, polarimetry can be performed either passively or actively.

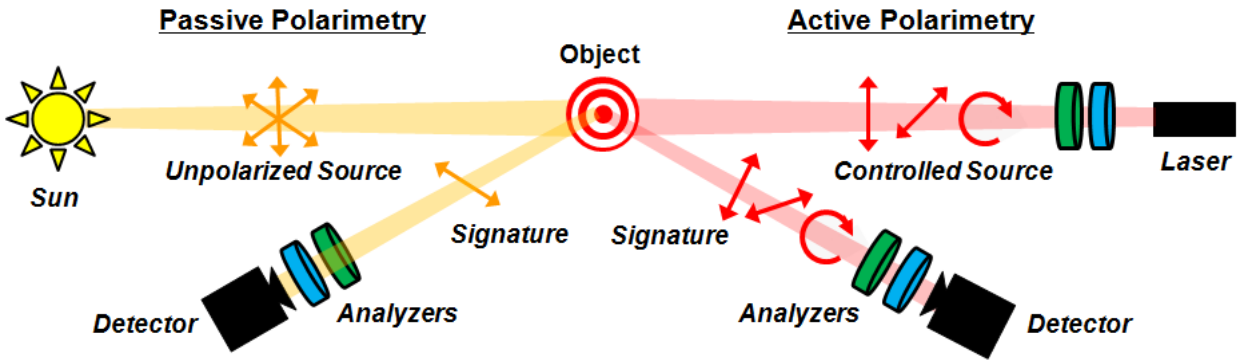

Figure 1 Illustration of passive vs. active polarimetry

With *passive* polarimetry, a target is illuminated by an external light source (e.g., the sun) and polarimetric measurements of the reflected light are taken using polarization analyzers placed in front of the detector [13, 14]. Meanwhile, with *active* polarimetry, a target is illuminated by a laser or other light source with a variable, but controlled, polarization state, and measurements are taken in the same manner [15, 16, 17, 18, 19]. Compared to the passive technique, active polarimetry is able to capture many more dimensions of a target's polarimetric signature, albeit at the cost of a more complex system, i.e., having to provide a light source with polarization control. In fact, active polarimetry enables one to estimate the complete polarimetric behavior of a material, as described by its Mueller matrix and associated polarimetric properties. The technical details of polarimetry are introduced briefly in the following subsections with references that contain more detailed descriptions.

2.1 Stokes Vector

The *polarization* state of light describes the orientation of its oscillating electrical field and can be conveniently represented by a 4 x 1 *Stokes vector* $\vec{S}$ as follows [20]:

$$\vec{S} = \begin{bmatrix} s_0 \\ s_1 \\ s_2 \\ s_3 \end{bmatrix} = \begin{bmatrix} I_{total} \\ I_H - I_V \\ I_{+45} - I_{-45} \\ I_{RC} - I_{LC} \end{bmatrix} \qquad \textbf{Eq. 1}$$

where $s_0 = I_{total}$ is the total intensity of the light, $s_1 = I_H - I_V$ is the intensity of all horizontally polarized components minus that of all vertically polarized component, $s_2 = I_{+45} - I_{-45}$ is the intensity of all +45º linearly polarized components minus that of all -45º linearly polarized components, and $s_3 = I_{RC} - I_{LC}$ is the intensity of all right-handed circularly polarized components minus that of all left-handed circularly polarized components.

2.2 Mueller Matrix

A material's effect on the polarization state of incident light can be quantified by a 4 x 4 real matrix called the *Mueller matrix M* as follows [20]:

$$M = \begin{bmatrix} m_{00} & m_{01} & m_{02} & m_{03} \\ m_{10} & m_{11} & m_{12} & m_{13} \\ m_{20} & m_{21} & m_{22} & m_{23} \\ m_{30} & m_{31} & m_{32} & m_{33} \end{bmatrix} \qquad \textbf{Eq. 2}$$

One can multiply the Stokes vector $\vec{S}^{in}$, describing the polarization state of incident light, by a material's Mueller matrix *M* to calculate the Stokers vector $\vec{S}^{out}$ describing the polarization state of the reflected (or transmitted) light.

$$M\vec{S}^{in} = \vec{S}^{out} \qquad \textbf{Eq. 3}$$

The Mueller matrix *M* can be converted to a *covariance matrix* Σ as follows [21]:

$$\Sigma = \frac{1}{2}\sum_{i=0}^{4}\sum_{j=0}^{4} m_{ij}\sigma_i \otimes \sigma_j \qquad \textbf{Eq. 4}$$

where ⊗ denotes the Kronecker product of matrices, and σ_i are the Pauli matrices defined as:

$$\sigma_1 = \begin{bmatrix} 1 & 0 \\ 0 & 1 \end{bmatrix} \qquad \sigma_2 = \begin{bmatrix} 1 & 0 \\ 0 & -1 \end{bmatrix} \qquad \sigma_3 = \begin{bmatrix} 0 & 1 \\ 1 & 0 \end{bmatrix} \qquad \sigma_4 = \begin{bmatrix} 0 & -i \\ i & 0 \end{bmatrix} \qquad \textbf{Eq. 5}$$

The covariance matrix Σ can also be expressed as:

$$\Sigma = V\Lambda V^{-1} \qquad \textbf{Eq. 6}$$

where Λ is a 4 x 4 diagonal matrix containing the four eigenvalues λ_i of Σ, and *V* is the corresponding matrix of unitary column eigenvectors v_i. The covariance matrix of any physically realizable (i.e., valid) Mueller matrix is guaranteed to be a positive semi-definite Hermitian (PSDH) matrix, which means that all four of Σ's eigenvalues are positive or zero. Thus, a condition for an arbitrary 4 x 4 real matrix to be a physically realizable Mueller matrix is that the eigenvalues of its associated covariance matrix meet this criterion:

Condition for Physical Realizability $\lambda_i \geq 0 \qquad i = 0, 1, 2, 3$ **Eq. 7**

2.3 Mueller Matrix Decomposition

A material's Mueller matrix can be decomposed to quantify its underlying polarimetric behavior. Any given material can exhibit a combination of three fundamental polarimetric behaviors [13]:

- *Diattenuation* is the preferential reflection (or transmittance) of certain polarization states over others.
- *Retardance* is the introduction of a phase shift between certain polarization states, by retarding one of their phases relative to the other.
- *Depolarization* is the conversion of polarized light into partially polarized or unpolarized light.

Lu and Chipman [22] describe the mathematics for decomposing a Mueller matrix into the product of three matrices corresponding to these fundamental behaviors:

$$M = M_\Delta M_R M_D \qquad \textbf{Eq. 8}$$

where M_D, M_R, and M_Δ are the 4 x 4 diattenuation, retardance, and depolarization factors, respectively. The general form of each matrix in Eq. 8 is:

$$M = \frac{1}{m_{00}}\begin{bmatrix} 1 & \vec{D}^T \\ \vec{P} & m \end{bmatrix} \qquad \textbf{Eq. 9} \qquad M_R = \begin{bmatrix} 1 & \vec{0}^T \\ \vec{0} & m_R \end{bmatrix} \qquad \textbf{Eq. 10}$$

$$M_D = T_u\begin{bmatrix} 1 & \vec{D}^T \\ \vec{D} & m_D \end{bmatrix} \qquad \textbf{Eq. 11} \qquad M_\Delta = \begin{bmatrix} 1 & \vec{0}^T \\ \vec{P}_\Delta & m_\Delta \end{bmatrix} \qquad \textbf{Eq. 12}$$

where $T_u = m_{00}^{-1}$ is the reflectivity (or transmittivity) for unpolarized light, $\vec{D}$ is the diattenuation vector, $\vec{P}$ and $\vec{P}_\Delta$ are the polarizance vectors of M and M_Δ , respectively, m, m_D, m_R, and m_Δ are the 3 x 3 sub-matrices of their respective parent matrices, and $\vec{0}$ is a 3 x 1 vector of zeros.

The procedure for decomposing a Mueller matrix as in Eq. 8 depends on whether the Mueller matrix is nondepolarizing (e.g., as with an ideal polarizer or waveplate) or depolarizing (e.g., as with rough surface). A necessary and sufficient condition for a Mueller matrix to be nondepolarizing is that its associated covariance matrix Σ (Eq. 4) only has one non-zero eigenvalue [23]:

Theoretical Condition for Nondepolarizing Behavior

$$\begin{aligned} \lambda_0 &> 0 \\ \lambda_i &= 0 \quad i = 1, 2, 3 \end{aligned} \qquad \textbf{Eq. 13}$$

If Eq. 13 is satisfied, the depolarization factor M_Δ in Eq. 8 can be set equal to the 4 x 4 identity matrix. Otherwise, M_Δ takes the general form of Eq. 12. Since matrix multiplication is not commutative, a Mueller matrix could also be decomposed with the factors permutated in five other possible sequences (e.g., $M = M_R M_D M_\Delta$), which can, in some cases, lead to a different interpretation of the material's behavior. We have restricted our analysis to the sequence in Eq. 8, since it is readily mathematically obtainable and has clear separation of the depolarizing (M_Δ) and nondepolarizing ($M_R M_D$) contributions [22]. In any case, the decomposition reveals an array of polarimetric properties describing the material's polarimetric behavior.

2.4 Polarimetric Properties

This paper highlights three specific polarimetric properties computed directly from the decomposed Mueller matrix. The first property is *diattenuation* (*D*), which is a dimensionless number (range 0 to 1) indicating how strongly the material reflects (or transmits) some polarization states relative to others [22]. A perfect diattenuator (e.g., an ideal linear polarizer) has a diattenuation of *D* = 1. Diattenuation is simply the magnitude of its diattenuation vector:

$$D = \left|\vec{D}\right| \qquad \textbf{Eq. 14}$$

The second property considered in this paper is *retardance (*R), which is the relative phase shift, in units of radians or degrees (range 0 to 180º), induced by the material onto its orthogonal eigenpolarizations [22]. A half-wave and quarter-wave plate have retardances of R = 180º and R = 90 º, respectively. The retardance is related to the trace (tr) of the retardance factor M_R as follows:

$$R = \cos^{-1}\left[\frac{\mathrm{tr}(M_R)}{2} - 1\right] \qquad \textbf{Eq. 15}$$

The third property of interest here is depolarization power (Δ), which is a dimensionless number (range 0 to 1) indicating how strongly the material depolarizes incident light [22]. An ideal depolarizer has a depolarization power of Δ = 1. The depolarization power of a material is related to the three eigenvalues λ_i^{Δ} of the sub-matrix m_{Δ} inside the depolarization factor M_{Δ} as follows:

$$\Delta = 1 - \frac{\left|\lambda_0^{\Delta}\right| + \left|\lambda_1^{\Delta}\right| + \left|\lambda_2^{\Delta}\right|}{3} \qquad \textbf{Eq. 16}$$

Many other polarimetric properties are also obtainable from the elements of the Mueller matrix and its decomposition [15, 16, 22]. For example, the polarizance $P = |\vec{P}|$ (range 0 to 1) describes how strongly the material converts unpolarized light into polarized light. All properties are potentially exploitable as a means of characterizing and identifying the material being measured. We chose to focus on the properties of diattenuation (D), retardance (R), and depolarization power (Δ) since they quantify the three fundamental polarimetric behaviors (Section 2.3).

2.5 Mueller Matrix Estimation

Polarimetry makes it possible to partially or completely determine a material or object's Mueller matrix and associated polarimetric properties. Whether polarimetry is done passively or actively, the governing mathematics, as depicted in Figure 2, are the same.

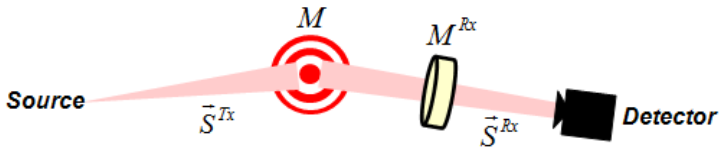

Figure 2 Depiction of polarimetry with Mueller calculus notation

If $\vec{S}^{Tx}$ is the Stokes vector of the light incident upon the material (whether from the sun or a laser), M is the Mueller matrix of the material being measured, and M^{Rx} is the Mueller matrix of the polarization analyzers placed in front of the detector, then the Stokes vector $\vec{S}^{Rx}$ of the light reaching the detector is given by applying Eq. 3 twice sequentially:

$$\vec{S}^{Rx} = M^{Rx} M \vec{S}^{Tx} \qquad \textbf{Eq. 17}$$

In our notation, $\vec{S}^{Tx}$ is the Stokes vector of Tx-polarized (e.g., H-polarized, or horizontally polarized) light that is "transmitted" (Tx) or sent to the material, while M^{Rx} is a Mueller matrix that "receives" (Rx) or passes the Rx-polarized component of the reflected light. Meanwhile, the Stokes vector $\vec{S}^{Rx}$ of the light that ultimately reaches the detector is actually inconsequential, since according to Eq. 1, the intensity I_{TxRx} measured by the detector is equal to the first element s_0^{Rx} of $\vec{S}^{Rx}$ (i.e., independent of polarization):

$$I_{TxRx} = s_0^{Rx} = \sum_{i=0}^{3} m_{0i}^{Rx} \sum_{j=0}^{3} s_j^{Tx} m_{ij} \qquad \textbf{Eq. 18}$$

where m_{0i}^{Rx} is element i of the first row of M^{Rx}, s_j^{Tx} is element j of $\vec{S}_{Tx}$, and m_{ij} is element (i, j) of M. If the 4 x 4 matrix M is reshaped to be a 16 x 1 vector $\vec{M}$, then Eq. 18 can be rewritten as a dot product:

$$I_{TxRx} = \vec{h}_{TxRx} \vec{M} \qquad \textbf{Eq. 19}$$

where the vectors $\vec{M}$ and $\vec{h}_{TxRx}$ are constructed as follows:

$$\vec{M} = \begin{bmatrix} m_{00} & m_{10} & m_{20} & m_{30} & m_{01} & \dots & m_{33} \end{bmatrix}^T \qquad \textbf{Eq. 20}$$

$$\vec{h}_{TxRx} = \begin{bmatrix} m_{00}^{Rx} s_0^{Tx} & m_{01}^{Rx} s_0^{Tx} & m_{02}^{Rx} s_0^{Tx} & m_{03}^{Rx} s_0^{Tx} & m_{00}^{Rx} s_1^{Tx} & \dots & m_{03}^{Rx} s_3^{Tx} \end{bmatrix} \qquad \textbf{Eq. 21}$$

Eq. 19 is the crux of polarimetry. By measuring $I_{Tx^n Rx^n}$ for N different Tx-Rx pairs, one can construct a system of N equations, each in the form of Eq. 19:

$$\vec{I} = H\vec{M}$$

$$\begin{bmatrix} I_{Tx^1 Rx^1} \\ I_{Tx^2 Rx^2} \\ \dots \\ I_{Tx^N Rx^N} \end{bmatrix} = \begin{bmatrix} \vec{h}_{Tx^1 Rx^1} \\ \vec{h}_{Tx^2 Rx^2} \\ \dots \\ \vec{h}_{Tx^N Rx^N} \end{bmatrix} \begin{bmatrix} m_{00} \\ m_{10} \\ \dots \\ m_{33} \end{bmatrix} \qquad \textbf{Eq. 22}$$

where the vectors $\vec{I}$ and matrix H are concatenations of the N measured intensities $I_{Tx^n Rx^n}$ and associated vectors $\vec{h}_{Tx^n Rx^n}$, respectively. Assuming a determined system (N linear independent equations, N unknowns), Eq. 22 can be solved as follows:

$$\vec{M} = H^{-1} \vec{I} \qquad \textbf{Eq. 23}$$

Depending on which elements of H are non-zero, the measured intensities $\vec{I}$ may be linear functions of some or all of the unknown Mueller matrix elements m_{ij}. With passive polarimetry, the sun always (nominally) transmits the same polarization state (Tx), specifically U, or "unpolarized" light, i.e., $\vec{S}^{Tx} = \vec{S}^{U} = [1\ 0\ 0\ 0]^{\mathrm{T}}$. Meanwhile, one can receive different polarization states (Rx) by changing the polarization analyzers in front of the detector, i.e., the matrix M^{Rx}. Applying Eq. 18, any measured intensities I_{URx} will only be functions of m_{00}, m_{10}, m_{20}, and m_{30}. By making N = 4 different Rx measurements, one can construct a system of 4 equations (Eq. 22) to solve for these 4 unknown elements. Thus, passive polarimetry can (at most) solve for the first column of M, which notably includes the material's polarizance vector $\vec{P}$ (by Eq. 9).

Meanwhile, with active polarimetry, one has individual control over both Tx and Rx, so measured intensities I_{TxRx} are generally functions of all 16 elements of M. Thus, by making N = 16 different Tx-Rx measurements, active polarimetry can solve for the entire Mueller matrix. If more than 16 measurements are made, the over-determined systems of equations can be solved with a least-squares estimator [24] .

2.6 Treatment of Experimental Mueller Matrices

In practice, Mueller matrix estimation is complicated by measurement errors. A noisy experimental Mueller matrix is unlikely to be physically realizable (Eq. 7), such that decomposition will yield nonsensical results. Cloude [21] provides a method for *filtering* an experimental Mueller matrix that does not satisfy Eq. 7 due to having a covariance matrix Σ (Eq. 4) with negative eigenvalues. Specifically, one can change all the negative eigenvalues to zero,

calculate the new covariance matrix using Eq. 6, and calculate the associated Mueller matrix using the inverse of Eq. 4. The "filtered" Mueller matrix is now, in some sense, the closest physically realizable Mueller matrix to the original noisy one, and can be legitimately decomposed as desired. Furthermore, the eigenvalue ratio γ of the largest (in magnitude) negative eigenvalue (of the original Σ) to the largest positive one can be calculated in decibels as follows:

$$\gamma = 10 \cdot \log_{10}\left(\frac{|\text{max negative } \lambda|}{\text{max positive } \lambda}\right) \qquad \textbf{Eq. 24}$$

The ratio γ is a measure of how close the original experimental Mueller matrix was to being physically realizable. Negative values of γ are expected, indicating that the negative eigenvalues are smaller (in magnitude) than the positive ones. Values of γ < -10 dB generally indicate experimental Mueller matrices that are very close to being physically realizable [21, 25].

Next, during decomposition (Eq. 8), one must determine whether the filtered, yet still noisy, Mueller matrix is nondepolarizing or depolarizing (Eq. 13). A noisy Mueller matrix is unlikely to perfectly satisfy Eq. 13 due to its covariance matrix Σ having more than one non-zero eigenvalue. However, an algorithm exists for declaring such a matrix to be nondepolarizing anyway [23, 26]. Let δ be a 4 x 4 matrix whose elements are the standard deviations of the noisy Mueller matrix elements. The noisy Mueller matrix can be declared nondepolarizing if:

Experimental Condition for Nondepolarizing Behavior $\qquad \sqrt{\lambda_1^2 + \lambda_2^2 + \lambda_3^2} \le \|\delta\|$ **Eq. 25**

where λ_1, λ_2, and λ_3 are the smallest three eigenvalues of Σ and $\|\delta\| = \sqrt{tr(\delta\delta')}$ is the Frobenius norm of δ. Eq. 25 checks whether the depolarizing components of the Mueller matrix are sufficiently in the noise. If Eq. 25 is satisfied, one can remove the negligible depolarizing components, similar to Cloude's [21] filtering method, by changing the smallest three eigenvalues to zero, calculating the new covariance matrix using Eq. 6, and calculating the associated Mueller matrix using the inverse of Eq. 4. The result is the closest nondepolarizing Mueller matrix to the original noisy one [23]. Decomposition (Eq. 8) of this new Mueller matrix can then be accomplished by first setting the depolarization factor M_Δ equal to the identity matrix. If Eq. 25 is not satisfied, the Mueller matrix is considered truly depolarizing and decomposition can be performed on the original matrix.

2.7 Polarimetric BRDF

When performing polarimetry on a material or object, the apparent Mueller matrix will depend on the illumination and viewing geometry, as quantified by the *Bidirectional Reflectance Distribution Function* (BRDF) [27, 28]. Nominally, a material's $BRDF(\theta_i,\phi_i,\theta_s,\phi_s)$, expressed in inverse steradians (sr^{-1}), is a function of the zenith angle θ_i (0 to 90°) and azimuth angle ϕ_i (-180 to 180°) of the incident beam, as well as those of the direction of scatter (θ_s and ϕ_s). More specifically, a material's BRDF also varies as a function of polarization, such that one would measure a different amount of scatter depending on the polarization state (Tx) of the incident light and the polarization component (Rx) of the reflected light that is passed through to the detector. Therefore, a material's polarimetric (or polarization-dependent) BRDF, written $BRDF(\theta_i,\phi_i,\theta_s,\phi_s,$Tx,Rx), can be computed from its geometry-dependent Mueller matrix, written $M(\theta_i,\phi_i,\theta_s,\phi_s)$, using Eq. 17 as follows:

$$BRDF(\theta_i,\phi_i,\theta_s,\phi_s,Tx,Rx) = M^{Rx} M(\theta_i,\phi_i,\theta_s,\phi_s)\vec{S}^{Tx} \qquad \textbf{Eq. 26}$$

where M^{Rx} and $\vec{S}^{Tx}$ are unitless, but $M(\theta_i,\phi_i,\theta_s,\phi_s)$ is given units of sr^{-1} [13]. By analogy with Eq. 22, one can make N = 16 different Tx-Rx measurements at geometry $(\theta_i,\phi_i,\theta_s,\phi_s)$ to compute the Mueller matrix $M(\theta_i,\phi_i,\theta_s,\phi_s)$ at that geometry. We sought to perform these very measurements using a bench-top polarimeter to investigate the polarimetric behavior of spacecraft materials.

3. EXPERIMENTAL SETUP AND PROCEDURE

We set up a bench-top polarimeter (Figure 3) to measure the polarimetric BRDF of material samples. The polarimeter uses a continuous-wave (CW) laser with a wavelength of λ = 1064 nm (Spectra-Physics® model Excelsior 1064-800). Several ground-based laser radars used for space surveillance also operate at 1064 nm using solid-state Nd:YAG lasers [7, 29]. The raw laser beam., which is horizontally polarized, passes through a half-wave (λ/2) plate and quarter-wave (λ/4) plate, which are independently rotated to control the polarization state (Tx) of the transmitted beam (i.e., $\vec{S}_{Tx}$ in Eq. 17). The beam (3 mm diameter) then encounters the material being measured. The light reflecting off the material passes through a λ/4 plate and λ/2 plate, which are independently rotated to control the polarization state (Rx) received by the detector (i.e., M^{Rx} in Eq. 17), followed by a fixed linear polarizer. A silicon detector (Thorlabs model PDA36A), combined with a lens giving a field-of-view of 1 cm on the material and an iris controlling the subtended solid angle (Ω), measures the intensity of the received light. To record a measurement, the laser is chopped at a frequency of 100 Hz and the detector's analog output is acquired using a lock-in amplifier (Princeton Applied Research Model 5209). The receiver assembly and target can be independently rotated to achieve arbitrary illumination and viewing geometries. All rotation stages (Newport® model PR50CC and RV120CCHL) are motorized and data collection is automated using Matlab®.

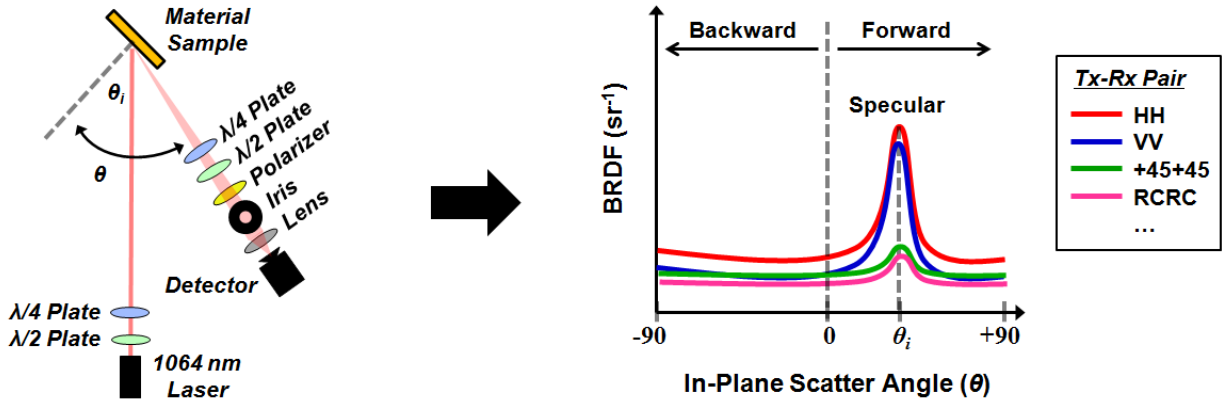

Figure 3 Diagram of bench-top polarimeter and hypothetical bistatic in-plane BRDF measurements

Our bench-top polarimeter measures a material's *bistatic in-plane* BRDF (Figure 3), i.e., the laser and receiver are separated in angle and scattered light is measured in the plane of incidence. The notation for an polarimetric in-plane BRDF can be simplified to $BRDF(\theta_i,\theta,Tx,Rx)$, where the azimuth arguments have been dropped and the scatter zenith angle θ_s has been replaced by θ (-90 to 90°). The backward, forward, and specular scatter regimes are defined by $\theta < 0$, $\theta > 0$, and $\theta = \theta_i$, respectively. At each geometry (θ_i, θ), the intensity I_{TxRx} of the scattered light is measured for each of the 16 Tx-Rx polarization pairs in Table 1, where horizontal, vertical, +45°, and right-hand circular polarizations have been abbreviated by H, V, +45, and RC, respectively.

Table 1 Intensity measurements for 16 Tx-Rx pairs

		Transmit Polarization (Tx)			
		H	**V**	**+45**	**RC**
Receive Polarization (Rx)	**H**	I_{HH}	I_{VH}	I_{+45H}	I_{RCH}
	V	I_{HV}	I_{VV}	I_{+4V}	I_{RCV}
	+45	I_{H+45}	I_{V+45}	I_{+45+45}	I_{RC+45}
	RC	I_{HRC}	I_{VRC}	I_{+45RC}	I_{RCRC}

The polarimetric BRDF is then calculated as follows [27]:

$$BRDF(\theta_i,\theta,Tx,Rx) = \frac{I_{TxRx}}{I_0 \Omega \cos\theta} \qquad \textbf{Eq. 27}$$

where I_0 is the intensity of the incident beam (which is the same for all Tx) and Ω = 500 μsr is the solid angle subtended by the iris in front of the detector. Each of the 16 measurements in Table 1 contributes a linearly independent equation in the form of Eq. 19, allowing us to solve for the geometry-dependent Mueller matrix $M(\theta_i,\theta)$ of the material being measured. We then filter $M(\theta_i,\theta)$ to ensure physical realizability (Section 2.6). After normalizing the matrix by the top-left element m_{00}, each filtered Mueller matrix is declared to be nondepolarizing if it satisfies Eq. 25 using δ = 0.02 (based on our measurements of reference samples [Section 3.1]), in which case the negligible depolarizing components are removed (Section 2.6). Finally, we decompose (in the form of Eq. 8) each filtered Mueller matrix to calculate its polarimetric properties as functions of θ_i and θ.

3.1 Verification

We verified the accuracy of our bench-top polarimeter in terms of its ability to measure (1) a reference sample with a known BRDF and (2) some common optical elements with known Mueller matrices. First, we measured the BRDF of a sample of Spectraflect®, a coating that is approximately Lambertian over the wavelength range from 350 to 2400 nm [30]. The manufacturer (Labsphere®) provided reference data on Spectraflect's in-plane BRDF for λ = 633 nm, incident angle θ_i = 30°, a Tx polarization of H (i.e., horizontally or "p" polarized), and an Rx polarization of U (or unpolarized, i.e., there was no polarization analyzer in front of the detector). For comparison, we measured the in-plane BRDF of Spectraflect® for λ = 1064 nm, θ_i = 30°, Tx polarization of H, and Rx polarizations of H and V (separately). Following Pickering's method [31], the sum of our measured BRDFs at HH and HV should be equivalent to the reference BRDF at HU. Spectral differences between our measurement (1064 nm) and the reference (633 nm) are expected to be negligible [30]. As plotted in Figure 4, our measurement falls within ±5% of the reference for the vast majority of scatter angles θ. This result verified our system's ability to accurately measure BRDF curves. Note that Spectraflect® has an approximately constant BRDF of π^{-1} = 0.32, as expected for a Lambertian surface [27].

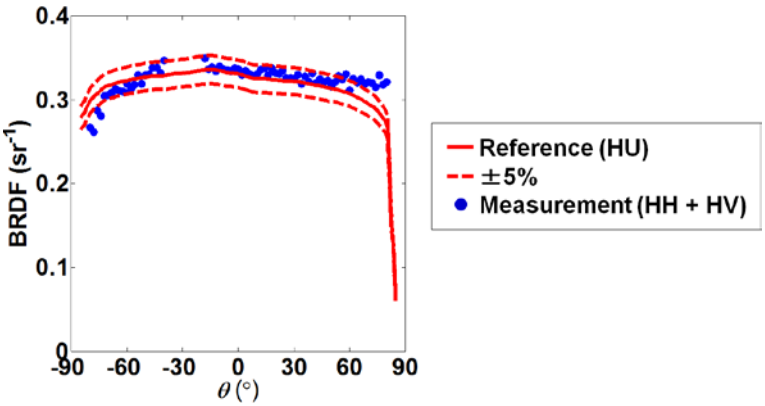

Figure 4 Measured vs. reference BRDF of Spectraflect® at θ_i = 30°

We also measured several common (transmissive) optical elements, where each element was illuminated at normal incidence and the detector assembly was positioned directly on the other side of the element. From the 16 prescribed measurements (Table 1), we calculated the Mueller matrix of each optical element. Despite measurement noise, all estimated Mueller matrices had associated eigenvalue ratios (Eq. 24) of γ < -18 dB, indicating that they were all extremely close to physically realizable matrices. Table 2 compares the estimated Mueller matrices (without any filtering) with the theoretical ones, after normalizing each by its top-left element m_{00}. The theoretical Mueller matrices contain only +1's, 0's, and -1's and the experimental Mueller elements are all within a margin of 0.02 relative to their respective theoretical values. Also included is the Mueller matrix of Spectraflect® at (θ_i,θ) = (30°, 0°), which is expected to be a strong depolarizer.

Table 2 Comparison of theoretical and experimental Mueller matrices of reference samples

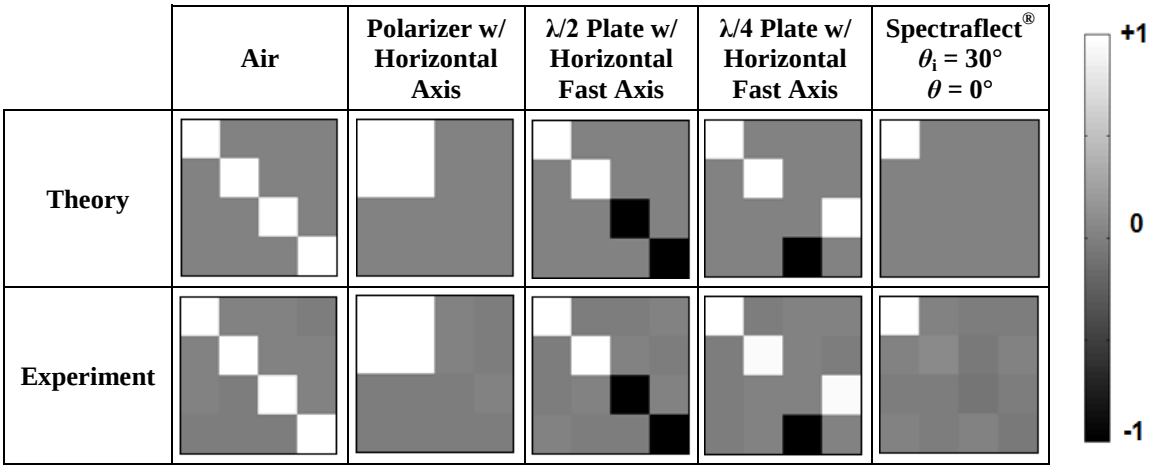

We then filtered (Section 2.6 and decomposed (Eq. 8) each experimental Mueller matrix and computed its polarimetric properties, including diattenuation (*D*, Eq.14), retardance (*R*, Eq. 15), and depolarization power (Δ, Eq. 16). Table 3 compares the experimental properties with the theoretical ones for each optical element, as well as for Spectraflect®. All the theoretical *D*'s and Δ's are 0 or 1, and all the theoretical *R*'s are 0 º, 90 º, or 180º. For the optical elements, the experimental *D*'s and Δ's are within 0.01 of their respective theoretical values, and the experimental *R*'s are within 4º. As expected, the Spectraflect® sample appeared highly depolarizing (Δ = 0.93), but we did not have a reference value for direct comparison. These results verified that we can use our bench-top polarimeter (Figure 3) to accurately estimate Mueller matrices, decompose them (Eq. 8), and compute their polarimetric properties (Eq. 14-16).

Table 3 Comparison of theoretical and experimental polarimetric properties of reference samples

Reference Sample	Diattenuation (*D*)		Retardance (*R*)		Depolarization Power (Δ)	
	Theory	Experiment	Theory	Experiment	Theory	Experiment
Air	0	0.00	0º	4º	0	0
Polarizer	1	0.99	0º	0º	0	0
λ/2 Plate	0	0.01	180º	179º	0	0
λ/4 Plate	0	0.01	90º	89º	0	0
Spectraflect®	Low	0.01	Low	-5°	High	0.93

3.2 Measurement of Spacecraft Materials

We used the bench-top polarimeter to measure the polarimetric BRDFs of the following materials and coatings commonly found on man-made satellites and debris, including:

- Glossy white paint (Aeroglaze® A276)
- Matte black paint (Aeroglaze® Z306)
- Black Kapton®
- Silver Teflon®
- Aluminum alloy (6061-T6)
- Titanium alloy (6Al-4V)

For each spacecraft material, we measured the in-plane BRDF for incident angles of θ_i = 15, 30, 45, 60 and 75° and scatter angles θ of -80 to 80° with 1° resolution around the expected specular (±10°) and 5° resolution elsewhere. A separate $BRDF(\theta_i,\theta,Tx,Rx)$ was measured for the 16 prescribed Tx-Rx polarization pairs (Table 1), allowing us to calculate each material's Mueller matrix and polarimetric properties as functions of θ_i and θ.

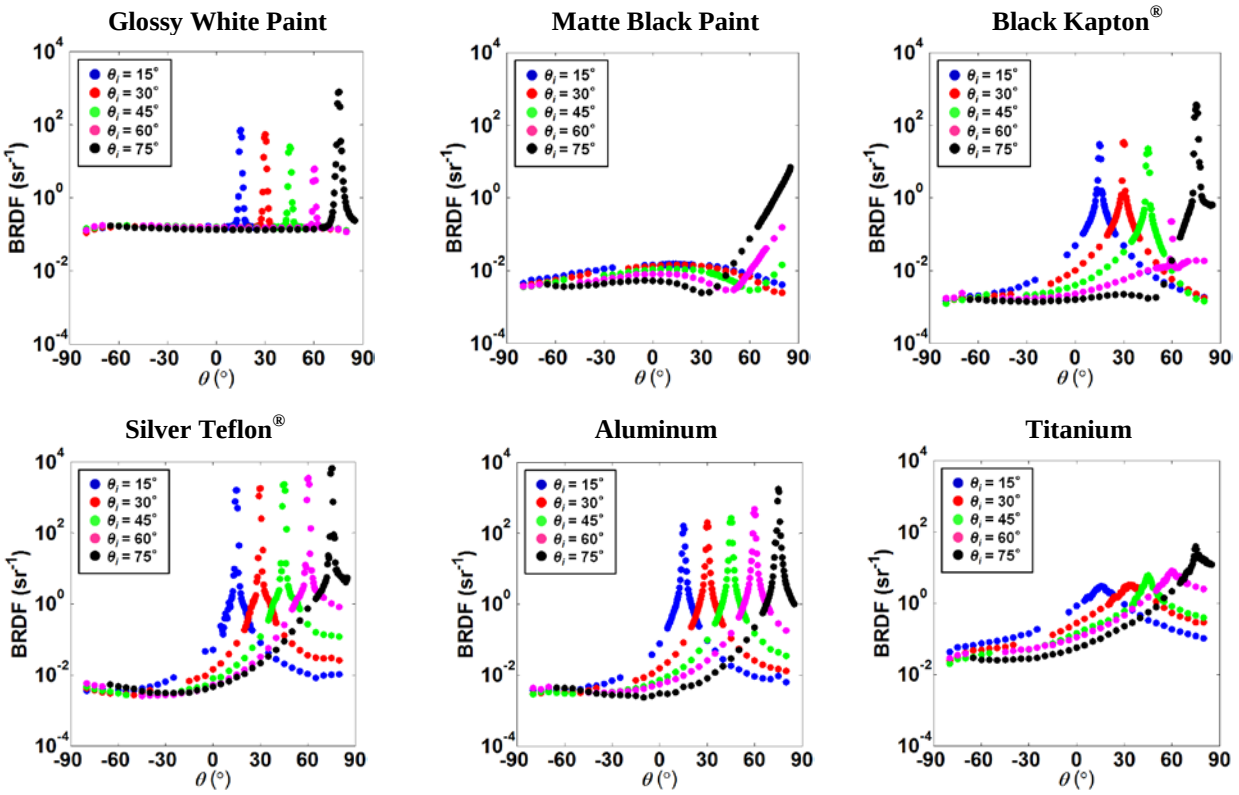

Figure 5 Measured in-plane BRDFs of spacecraft materials at polarization HH

4. RESULTS AND ANALYSIS

Here we present the results of our experiments on the spacecraft materials introduced above. We first consider the in-plane BRDF measured for each spacecraft material for a single polarization pair. Figure 5 shows each spacecraft material's in-plane BRDF (vs. θ) measured at polarization pair HH and several incident angles θ_i. All materials have a dominant specular component at $\theta = \theta_i$, with the exception of the matte black paint, which is mostly diffuse but with significantly increased forward scatter for high incident angles.

We next consider the ensemble of 16 polarimetric in-plane BRDFs measured for a single material and incidence angle θ_i. Figure 6 shows such an ensemble for glossy white paint at $\theta_i = 60°$. Also shown is the computed Mueller matrix at a diffuse point ($\theta = -30°$) and specular point ($\theta = 60°$), each normalized by its top-left element m_{00}. The Mueller matrix at $\theta = -30°$ is visually recognizable as a strong depolarizer (e.g., see Sepctraflect® in Table 2), such that all 16 BRDFs are of roughly equal magnitude at this point. By contrast, the Mueller matrix at the specular point is that of a vertical linear polarizer, such that vertically (V) polarized incident light is preferentially reflected over horizontally (H) polarized incident light. Indeed, at $\theta = 60°$ the BRDF at VV is significantly higher than the BRDF at HH (see inset). This diattenuating behavior at the specular point is expected from Fresnel's equation for a moderately high θ_i, which dictates that "s" polarized light (i.e., equivalent to V here) will be reflected more than "p" (or H) polarized light [13].

Finally, using the 16 polarimetric BRDFs measured for each material, we computed the materials' Mueller matrices and polarimetric properties as functions of θ_i and θ. All estimated Mueller matrices had associated eigenvalue ratios (Eq. 24) of $\gamma < -10$ dB, indicating that they were very close to physically realizable matrices. Figure 7 and Figure 8 (at end of paper) show each material's diattenuation (D), retardance (R), and depolariazation power (Δ) as functions of θ for all θ_i. The plots reveal some notable trends in the polarimetric signatures of the materials, as summarized in Table 4 according the direction of scatter: backward ($\theta < 0$), forward ($\theta > 0$), and specular ($\theta = \theta_i$). All materials exhibited mostly low diattenuation ($D < 0.5$) in the back scatter direction. However, in the forward scatter direction (including the specular), the metallic surfaces (i.e., titanium, aluminum, and silver Teflon®) continued exhibiting D

< 0.5, while the two paints and Kapton® had the full range of diattenuaton (D = 0 to 1). In terms of retardance, the silver Teflon® uniquely exhibited a finite range (R = 30 to 120º) in all scatter directions, while all other materials acted as mirrors (R = 180º) in the back scatter direction and had the full range of behavior (R = 0 to 180º) in the forward scatter direction. Finally, in terms of depolarization power, the glossy white paint was a nearly perfect depolarizer ($\Delta \approx 1$) in the back-scatter direction, but sharply lost depolarization power ($\Delta = 0$) at specular reflection. All other materials were mostly weak depolarizers ($\Delta < 0.5$) in all directions, except that silver Teflon® and aluminum exhibit moderately high depolarization power ($0.5 < \Delta < 0.8$) in the back scatter direction.

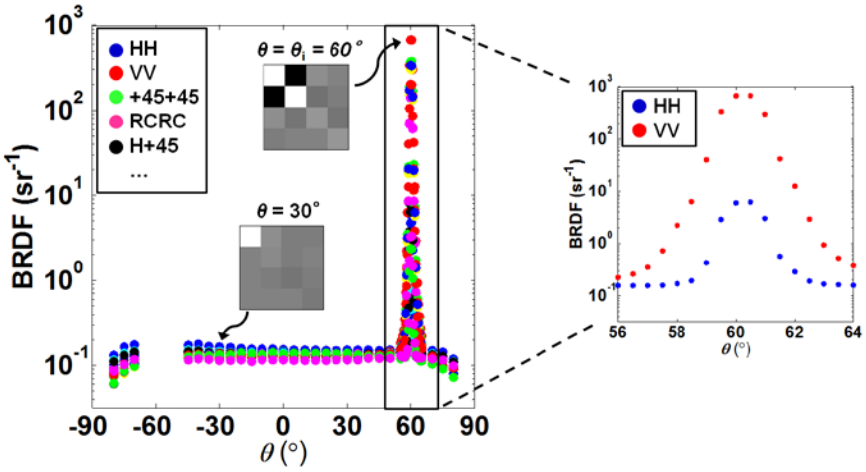

Figure 6 Measured in-plane BRDF (θ_i = 60°) of white paint at 16 polarizations (left) and HH & VV (right)

Table 4 Trends in polarimetric properties

<table>
<tr><th rowspan="2">Spacecraft Material</th><th colspan="3">Diattenuation (D)</th><th colspan="3">Retardance (R)</th><th colspan="3">Depolarization Power (Δ)</th></tr>
<tr><th>Back (θ < 0)</th><th>Forw. (θ > 0)</th><th>Specular ($\theta = \theta_i$)</th><th>Back (θ < 0)</th><th>Forw. (θ > 0)</th><th>Specular ($\theta = \theta_i$)</th><th>Back (θ < 0)</th><th>Forw. (θ > 0)</th><th>Specular ($\theta = \theta_i$)</th></tr>
<tr><td>Glossy White Paint</td><td rowspan="3">< 0.5</td><td rowspan="3">0 - 1</td><td rowspan="3">0 – 1*</td><td rowspan="4">180º</td><td rowspan="2">0 - 180º</td><td rowspan="2">0 - 180º*</td><td>1</td><td>0 - 1</td><td rowspan="5">0*</td></tr>
<tr><td>Matte Black Paint</td><td rowspan="2">< 0.5</td><td rowspan="3">< 0.5</td></tr>
<tr><td>Black Kapton®</td></tr>
<tr><td>Titanium</td><td colspan="3" rowspan="3">< 0.5</td><td colspan="2">> 40º</td><td rowspan="3">0 - 1</td></tr>
<tr><td>Aluminum</td><td colspan="2">> 70º</td></tr>
<tr><td>Silver Teflon®</td><td colspan="2">30 to 120º</td></tr>
</table>

∗ Specular trends do not apply to matte black paint

5. DISCUSSION

Our experimental results (Table 4) demonstrate that common spacecraft materials have distinguishing polarimetric properties, suggesting that orbital debris fragments may exhibit polarimetric signatures indicative of their constituent materials. A polarimetric laser radar could exploit this phenomenon using active polarimetry. Specifically, the laser radar could interrogate a debris fragment by sequentially transmitting and receiving different pairs of Tx and Rx polarization states, and estimating the debris fragment's effective Mueller matrix and polarimetric properties. A classification algorithm could then use the estimated properties to identify (or categorize) the debris fragment's constituent materials. If the debris fragment's constituent materials can be accurately identified, then one could also infer its density, mass, origin, and other characteristics of interest [2].

The ultimate utility of active polarimetry for space surveillance will depend on several outstanding issues concerning phenomenology, system architecture, and algorithm development. In terms of phenomenology, although we have measured the polarimetric BRDFs of spacecraft materials in the laboratory, we have not yet considered the

signal expected from non-resolved (i.e., in angle) orbital debris fragments. Among other factors, the amount of laser light reflecting from a debris fragment will depend on its shape (i.e., surface geometry) and the polarimetric BRDF of its surface materials at the operating wavelength. The architecture of the laser radar will also affect the measured signal. For instance, one would expect different phenomenology for a bistatic system (i.e., separated source and sensor) compared to a monostatic one (i.e., co-located source and sensor) [17, 18]. Meanwhile, a ground-based system, as opposed to a space-based one [32], must account for atmospheric attenuation and effects on the transmitted and received polarization states. For any system, errors in the estimated Mueller matrix and polarimetric properties will blur the distinction between polarimetric signatures [33]. Algorithms will be needed to distinguish between noisy polarimetric behaviors and then identify or categorize the measured object [18, 26]. The optimal classification scheme may need to fuse polarimetric, spectral, radar, and orbital features. Future consideration of active polarimetry for space surveillance should include analysis of these issues in more detail.

6. CONCLUSION

To investigate the potential utility of active polarimetry for orbital debris characterization, we used a bench-top polarimeter to measure the polarimetric BRDF of several common spacecraft materials. These measurements allowed us to estimate each material's Mueller matrices and polarimetric properties as functions of the incident angle and (bistatic) in-plane scatter angle. The materials exhibited notable trends in their polarimetric behaviors. All the materials exhibited mostly weak diattenuation ($D < 0.5$) in all scatter directions, except for Kapton® and the two paints ($D > 0.5$ in the forward scatter direction). In terms of retardance (R), silver Teflon® exhibited a finite range of values (R = 30 to 120º) in all directions, while the other materials acted as mirrors (R = 180º) in the back scatter direction and had the full range of behavior (R = 0 to 180º) in the forward scatter direction. Finally, in terms of depolarization power (Δ), glossy white paint was a nearly perfect depolarizer ($\Delta \approx 1$) in the back scatter direction, but sharply lost depolarization power ($\Delta = 0$) at specular reflection. All other materials were mostly weak depolarizers ($\Delta < 0.5$) in all scatter directions. Pending further analysis, our findings suggest that a laser radar may be able to make active polarimetric measurements to help remotely identify and characterize debris fragments. In future work, we plan to explore polarimetric phenomenology in more detail, including monostatic measurements of spacecraft materials (as well as meteorite samples) and simulation of non-resolved polarimetric signatures.

REFERENCES

[1] Inter-Agency Space Debris Coordination Committee, *Stability of the Future LEO Environment,* 2013.

[2] N. J. Johnson and D. S. McKnight, Artificial Space Debris, Malabar, FL: Krieger Publishing Company, 1991.

[3] Inter-Agency Space Debris Coordination Committee, *Space Debris Mitigation Guidelines*, 2007.

[4] D. J. Kessler and B. G. Cour-Palais, "Collision frequency of artificial satellites: the creation of a debris belt," *Journal of Geophysical Research*, vol. 83, no. A6, pp. 2637-2646, 1978.

[5] J. C. Liou, "An active debris removal parametric study for LEO environment remediation," *Advances in Space Research,* vol. 47, pp. 1865-1876, 2011.

[6] J. W. Campbell, "Using lasers in space," 2000.

[7] J. D. Eastment, D. N. Ladd and C. J. Walden, "Technical description of radar and optical sensors contributing to joint UK-Australian satellite tracking, data fusion and cueing experiment," in *Advanced Maui Optical and Space Surveillance Technologies Conference*, Wailea, HI, 2014.

[8] G. C. Giakos, R. H. Picard and P. D. Dao, "Superresolution multispectral imaging polarimetric space surveillance LADAR sensor design architectures," in *Remote Sensing*, 2008.

[9] J. Sang, J. C. Bennett and C. Smith, "Experimental results of debris orbit predictions using space tracking data from Mt. Stromlo," *Acta Astronautica,* vol. 102, pp. 258-268, 2014.

[10] Z.-P. Zhang, F.-M. Yang, H.-F. Zhang, Z.-B. Wu, J.-P. Chen, P. Li and W.-D. Meng, "The use of laser ranging to measure space debris," *Research in Astronomic and Astrophysics.*

[11] B. Greene, G. Yuo and M. Christ, "Laser tracking of space debris," in *13th International Workshop n Laser Ranging*, Washington, D.C., 2002.

[12] K. Rochford, "Polarization and Polarimetry," *National Institute of Standards and Technology.*

[13] J. R. Schott, Fundamentals of Polarimetric Remote Sensing, Bellingham, WA: SPIE Press, 2009.

[14] J. S. Tyo, D. L. Goldstein, D. B. Chenault and J. A. Shaw, “Review of passive imaging polarimetry for remote,” *Applied Optics*, vol. 45, no. 22, pp. 5453-5469, 2006.

[15] J. L. Pezzaniti and R. A. Chipman, "Mueller matrix imaging polarimetry," *Optical Engineering*, vol. 34, no. 6, 1995.

[16] P. Refregier, F. Goudail and N. Roux, "Estimation of the degree of polarization in active coherent imagery by using the natural representation," *Journal of the Optical Society of America A*, vol. 21, no. 12, 2004.

[17] S. Breugnot and P. Clemenceau, “Modeling and performance of polarimetric active imager at 806nm,” *Optical Engineering*, vol. 30, no. 10, pp. 2681-2688, 2000.

[18] C. S. Chun and F. A. Sadjadi, “Polarimetric laser radar target classification,” *Optics Letters*, vol. 30, no. 14, pp. 1806-1808, 2005.

[19] J. S. Baba, J.-R. Chung, A. H. DeLaughter, B. D. Cameron and G. L. Cote, “Development and calibration of a m automated Mueller matrix polarization imaging system,” *Journal of Biomedical Optics*, vol. 7, no. 3, pp. 341-349, 2002.

[20] E. Hecht, Optics, Boston: Pearson, 2002.

[21] S. R. Cloude, "Conditions for the physical realisability of matrix operatrors in polarimetry," in *SPIE Polarization Considerations for Optical Systems II*, 1989.

[22] S.-Y. Lu and R. A. Chipman, "Interpretation of Mueller matrices based on polar decomposition," *Journal of the Optical Society of America A*, vol. 13, no. 5, pp. 1106-1113, 1996.

[23] F. Le. Roy-Brehonnet, B. Le Jeune, P. Y. Gerligand, J. Cariou and J. Lotrian, "Analysis of depolarizing optical targets by Mueller matrix formalism," *Pure & Applied Optics*, vol. 6, pp. 385-404, 1997.

[24] G. Strang, Introduction to Applied Mathematics, Wellesley, MA: Wellesley-Cambridge Press, 1986.

[25] D. Goldstein, Polarization Light, New York: Marcel Decker, Inc., 2003.

[26] F. Boulvert, G. Le Brun, B. Le Jeune, J. Cariou and L. Martin, "Decomposition algorithm of an experimental Mueller matrix," *Optics Communications*, vol. 282, no. 5, pp. 692-704, 2009.

[27] J. C. Stover, Optical Scattering: Measurement and Analysis, 1995.

[28] F. E. Nicodemus, "Directional reflectance and emissivity of an opaque surface," *Applied Optics*, vol. 4, no. 7, pp. 767-773, 1965.

[29] A. B. Gschwendtner and W. E. Keicher, "Development of coherent laser radar at Lincoln Laboratory," *Lincoln Laboratory Journal*, vol. 12, no. 2, 2000.

[30] Labsphere, Inc., 2015. [Online]. Available: http://www.labsphere.com.

[31] J. E. Solomon, "Polarization imaging," *Applied Optics*, vol. 20, no. 9, pp. 1537-1544, 1981.

[32] S. V. Garnov, A. V. Moiseeva, P. Y. Nosatenko, V. N. Fomin and A. B. Tserevitinov, "Estimation of the characteristics of a promisiing orbital lidar for space debris monitoring".

[33] D. M. Hayes, "Error propagation in decomposition of Mueller matrices," in *SPIE: Polarization: Measurement, Analysis, and Remote Sensing*, 1997.

[34] N. N. Smirnov, Ed., Space Debris: Hazard Evaluation and Mitigation, New York: Taylor and Francis, 2002.

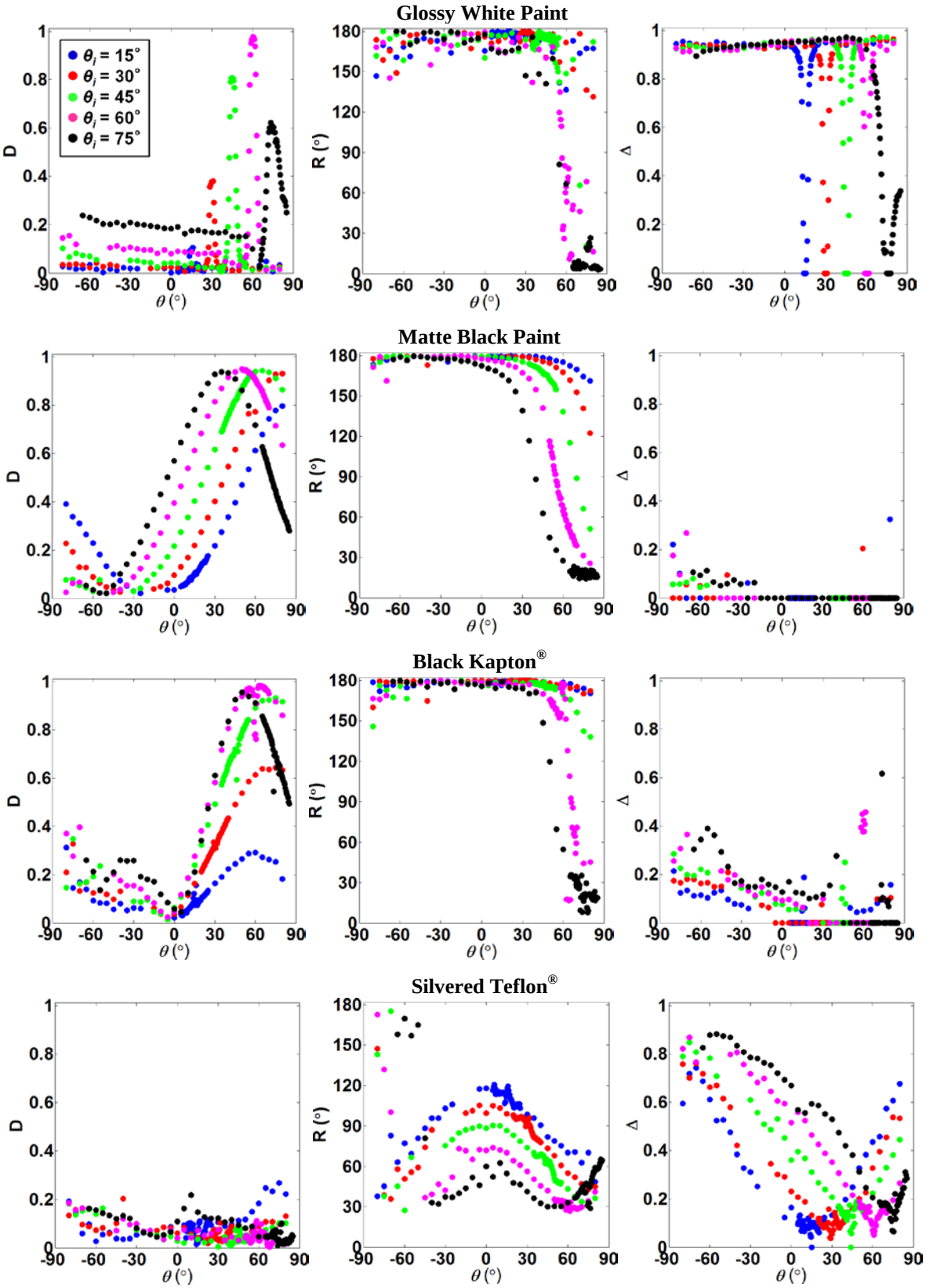

Figure 7 Polarimetric properties (*D*, *R*, and Δ) of spacecraft materials vs. (θ_i, θ)

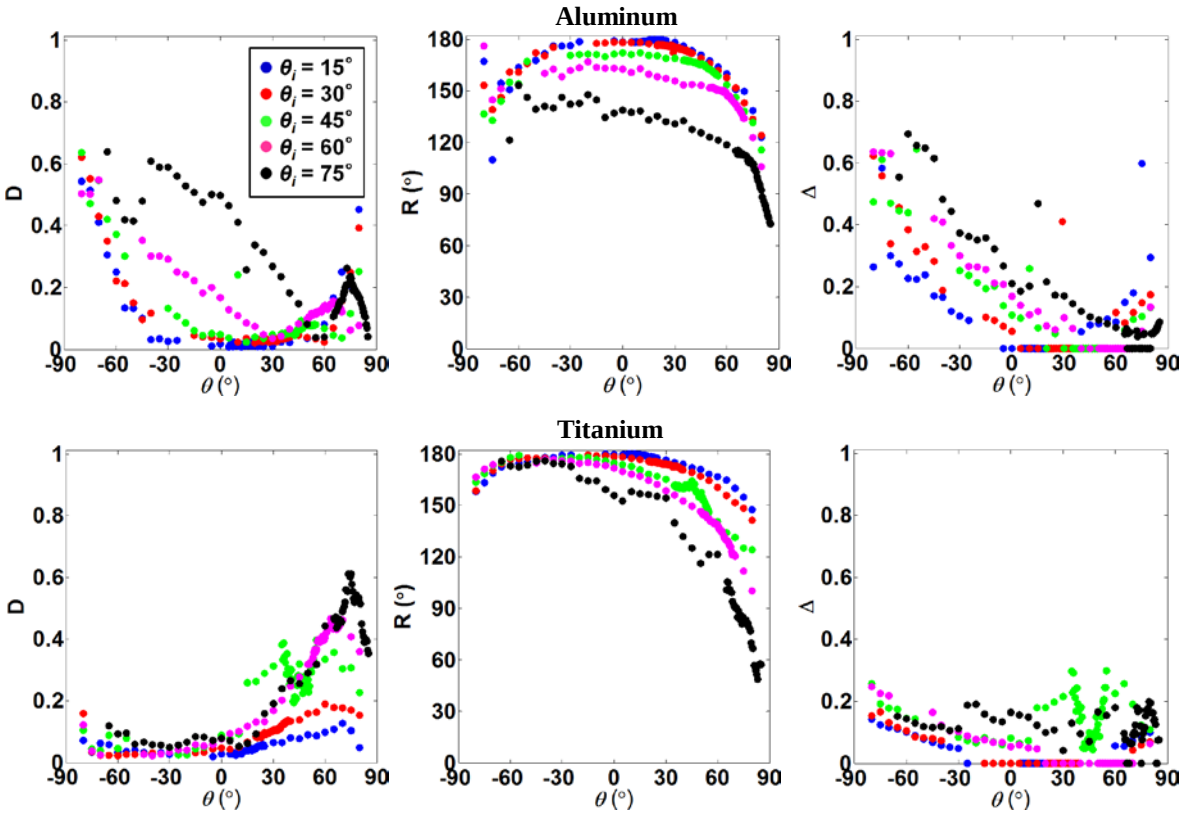

Figure 8 Polarimetric properties (*D*, *R*, and Δ) of spacecraft materials vs. (θ_i, θ)